A new multiscale discontinuous Galerkin method for the one-dimensional stationary Schrödinger equation

Bo Dong*, Chi-Wang Shu† and Wei Wang‡

Abstract

In this paper, we develop and analyze a new multiscale discontinuous Galerkin (DG) method for one-dimensional stationary Schrödinger equations with open boundary conditions which have highly oscillating solutions. Our method uses a smaller finite element space than the WKB local DG (WKB-LDG) method proposed in [18] while achieving the same order of accuracy with no resonance errors. We prove that the DG approximation converges optimally with respect to the mesh size h in L^2 norm without the typical constraint that h has to be smaller than the wave length. Numerical experiments were carried out to verify the second order optimal convergence rate of the method and to demonstrate its ability to capture oscillating solutions on coarse meshes in the applications to Schrödinger equations.

Key words: discontinuous Galerkin method, multiscale method, Schrödinger equation

*Email: bdong@umassd.edu. Department of Mathematics, University of Massachusetts Dartmouth, North Dartmouth, MA 02747.

†E-mail: shu@dam.brown.edu. Division of Applied Mathematics, Brown University, Providence, RI 02912.

‡E-mail: weiwang1@fiu.edu. Department of Mathematics & Statistics, Florida International University, Miami, FL, 33199.

1 Introduction

In this paper, we propose a new multiscale discontinuous Galerkin (DG) method for the following one-dimensional second order elliptic equation

$$-\varepsilon^2 u'' - f(x)u = 0, \tag{1.1}$$

where $\varepsilon > 0$ is a small parameter and $f(x)$ is a real-valued smooth function independent of ε. The solution to this equation for positive f is a wave function with the wave number $\frac{\sqrt{f(x)}}{\varepsilon}$.

One application of this type of equation is the stationary Schrödinger equation in the modeling of quantum transport in nanoscale semiconductors [5, 14, 18]

$$\begin{cases} -\frac{\hbar^2}{2m}\varphi''(x) - qV(x)\varphi(x) = E\varphi(x) \quad \text{on } [a,b] \\ \hbar\varphi'(a) + \boldsymbol{i}p(a)\varphi_p(a) = 2\boldsymbol{i}p(a), \quad \hbar\varphi_p'(b) = \boldsymbol{i}p(b)\varphi(b), \end{cases} \tag{1.2}$$

with $\varepsilon = \dfrac{\hbar}{\sqrt{2mE}}$ and $f(x) = 1 + \dfrac{qV(x)}{E}$ in Equation (1.1). Here $\hbar$ is the reduced Plank constant, m is the effective mass (assumed to be constant), q is the elementary positive charge of the electron, $V(x)$ is the total electrostatic potential in the device, E is the injection energy, $p(x) = \sqrt{2m(E + qV(x))}$ is the momentum, and the solution φ is a wave function. The quantum mechanical picture of the equation describes an electron injected from $x = a$ with an energy E, and partially transmitted or reflected by the potential V. The imposed open boundary conditions are the so-called quantum transmitting boundary conditions, see [13]. In the modeling of quantum transport, the Schrödinger equation is coupled with a Poisson equation in order to compute the self-consistent potential. In this paper, the total potential $V(x)$ is considered to be a known function as the coupling with the Poisson equation does not change our DG method for the Schrödinger equation.

When the electron has high energy E, i.e. ε is very small, the solution to the Schrödinger equation will be highly oscillating. Standard numerical methods require very fine meshes to resolve such oscillations. As a result, the computational cost is tremendous in order to simulate quantum transport in nano devices since millions of Schrödinger equations need to be solved. The design of efficient multiscale numerical methods which produce accurate approximations of the solutions on coarse meshes is a formidable mathematical challenge. Note that when the energy E is small, such that $E + qV < 0$

(i.e. $f < 0$), the solution is non-oscillatory. Thus we mainly focus on the challenging case of $f(x) \geq \tau > 0$ and $0 < \varepsilon \ll 1$.

A lot of work has been dedicated to the development of efficient methods for solving stationary Schrödinger equations, such as [15, 16, 5, 4, 14, 18, 3]. In [5], Ben Abdallah and Pinaud proposed a multiscale continuous finite element method for the one-dimensional Schrödinger equation (1.2). Using WKB asymptotics [6], they constructed continuous WKB basis functions, which can better approximate highly oscillating wave functions than the standard polynomial interpolation functions so that the computational cost is significantly reduced. This method was analyzed in [14] and second order convergence was shown independent of the wave length. One limitation of the method is that it is difficult to be generalized to general two-dimensional devices due to the difficulty in extending such continuous multiscale basis functions to two dimensions.

Different from continuous finite element methods, DG methods [2, 9, 8] do not enforce continuity at element interfaces, which makes them feasible to be extended to multidimensional devices. Multiscale DG methods with non-polynomial basis functions have been developed and studied in the literature, including [1, 19, 11, 20, 7, 12, 18, 17, 21]. In [18], Wang and Shu proposed a local DG method with WKB basis (WKB-LDG) for solving the one-dimensional stationary Schrödinger equation (1.2) in the simulation of resonant tunneling diode model. Numerical tests showed that the WKB-LDG method using piecewise exponential basis functions can resolve solutions on meshes that are coarser than what the standard DG with polynomial basis requires. However, no convergence analysis was done for this method.

In this paper, we propose and analyze a new multiscale DG method for the stationary Schrödinger equation. Our method is different from the WKB-LDG method in [18] in two aspects. First, we use a smaller finite element space than that of the WKB-LDG method to achieve the same order of convergence and reduce the resonance errors. Second, in the definition of the numerical traces we penalize the jumps using imaginary parameters, so our method is not an LDG method when the penalty parameters are nonzero.

The analysis of the multiscale DG method is challenging. Due to the strong indefiniteness of the Schrödinger equation with positive f, it is hard to establish stability estimates for finite element solutions. When an energy argument is used, one only gets a Gårding-type equality instead of the energy equality. Moreover, there is a typical mesh constraint $h \lesssim \varepsilon$ for numerically resolving highly oscillating solutions using finite element methods. In order to

prove convergence results for both $h \gtrsim \varepsilon$ and $h \lesssim \varepsilon$ cases, special projection results and inverse inequalities are needed.

A novel and crucial part of our analysis is Theorem 3.1 for the L^2 projection onto the space of piecewise exponential functions. For general H^1 functions, the projection requires that the mesh size is small enough, at least comparable to the wave length, to have a second-order approximation. But for the oscillating solutions of the model problem and the corresponding dual problem, we show that the second-order approximation can be obtained even if the mesh size h is larger than the wave length. Thanks to this projection result, we are able to derive error estimates without assuming $h \lesssim \varepsilon$. We first use an energy argument to get a Gåding type equality. The fact that the penalty parameters are imaginary allows us to estimate jumps of the errors at cell interfaces; similar idea has been used in [10]. Then we apply a duality argument to estimate the error in the interior of the mesh, and the error estimate at cell interfaces allows us to control the boundary terms without using inverse inequality and losing convergence orders.

The paper is organized as follows. In Section 2, we define our multiscale DG method for the stationary Schrödinger equation. In Section 3, we state and discuss the main results. The detailed proofs are given in Section 4. We display the numerical results in Section 5 to verify our error estimates and compare our method with the LDG method using piecewise linear and quadratic functions and the WKB-LDG method in [18]. Finally, we conclude in Section 6.

2 Multiscale DG method: The Methodology

2.1 The DG formulation

The model problem we investigate in this paper can be written as follows:

$$\begin{cases} -\varepsilon^2 u'' - f(x)u = 0, \quad x \in [a,b], \\ u'(a) + \boldsymbol{i}k(a)\,u(a) = 2\boldsymbol{i}k(a), \quad u'(b) - \boldsymbol{i}k(b)\,u(b) = 0, \end{cases} \tag{2.1}$$

where $k(x) = \dfrac{\sqrt{f(x)}}{\varepsilon}$ is the wave number.

In order to define a DG method for the elliptic equation (2.1), we rewrite it into a system of first order equations

$$q - \varepsilon u' = 0, \quad -\varepsilon q' - f(x)u = 0 \tag{2.2a}$$

with the boundary conditions

$$q(a) + \boldsymbol{i}\sqrt{f_a}\, u(a) = 2\boldsymbol{i}\sqrt{f_a}, \quad q(b) - \boldsymbol{i}\sqrt{f_b}\, u(b) = 0, \tag{2.2b}$$

where $f_a = f(a)$ and $f_b = f(b)$.

Let $I_j = (x_{j-\frac{1}{2}}, x_{j+\frac{1}{2}}), j = 1, \ldots, N$, be a partition of the domain, $x_j = \frac{1}{2}(x_{j-\frac{1}{2}} + x_{j+\frac{1}{2}})$, $h_j = x_{j+\frac{1}{2}} - x_{j-\frac{1}{2}}$ and $h = \max_{j=1,\cdots,N} h_j$. Let $\Omega_h := \{I_j : j = 1, \ldots, N\}$ be the collection of all elements, $\partial\Omega_h := \{\partial I_j : j = 1, \ldots, N\}$ be the collection of the boundaries of all elements, $\mathscr{E}_h := \{x_{j+\frac{1}{2}}\}_{j=0}^{N}$ be the collection of all the cell interfaces, and $\mathscr{E}_h^{oi} := \{x_{j+\frac{1}{2}}\}_{j=1}^{N-1}$ be the collection of all interior cell interfaces.

The weak formulation of a standard DG method for Equation (2.2a) is to find approximate solutions u_h and q_h in a finite element space V_h such that

$$(q_h, w)_{\Omega_h} + (\varepsilon u_h, w')_{\Omega_h} - \langle \varepsilon \widehat{u}_h, w\, \boldsymbol{n}\rangle_{\partial\Omega_h} = 0 \tag{2.3a}$$

$$(\varepsilon q_h, v')_{\Omega_h} - \langle \varepsilon \widehat{q}_h, v\, \boldsymbol{n}\rangle_{\partial\Omega_h} - (f(x)u_h, v)_{\Omega_h} = 0. \tag{2.3b}$$

for all test functions $v_h, w_h \in V_h$. Here, we have used the notation

$$(\varphi, v)_{\Omega_h} := \sum_{j=1}^{N} (\varphi, v)_{I_j}, \quad \langle \psi, w\, \boldsymbol{n}\rangle_{\partial\Omega_h} := \sum_{j=1}^{N} \langle \psi, w\, \boldsymbol{n}\rangle_{\partial I_j},$$

where

$$\begin{aligned} (\varphi, v)_{I_j} &= \int_{I_j} \varphi(x)\overline{v}(x)\, dx, \\ \langle \psi, w\, \boldsymbol{n}\rangle_{\partial I_j} &= \psi(x_{j+\frac{1}{2}})\overline{w}(x_{j+\frac{1}{2}}) - \psi(x_{j-\frac{1}{2}})\overline{w}(x_{j-\frac{1}{2}}), \end{aligned}$$

where $\overline{v}$ is the complex conjugate of v and $\boldsymbol{n}$ is the unit outward normal vector. For $I_j = (x_{j-\frac{1}{2}}, x_{j+\frac{1}{2}})$, we assume $\boldsymbol{n}(x_{j-\frac{1}{2}}) = -1$ and $\boldsymbol{n}(x_{j+\frac{1}{2}}) = 1$. The numerical traces $\widehat{u}_h$ and $\widehat{q}_h$ will be defined in the next subsection.

The finite element space V_h contains functions which are discontinuous across cell interfaces. For standard DG methods, these functions are piecewise polynomials. For our proposed multiscale DG method, the basis functions are constructed to be non-polynomial functions which incorporate the small scales to better approximate the oscillating solutions, and we will give more details in Section 2.3. Since the functions in V_h are allowed to have discontinuities at cell interfaces $x_{j+\frac{1}{2}}$, we use $v^-(x_{j+\frac{1}{2}})$ and $v^+(x_{j+\frac{1}{2}})$ to refer to the left and right limits of v at $x_{j+\frac{1}{2}}$, respectively.

2.2 The numerical traces

The choices of numerical traces are essential for the definition of DG methods, and different numerical traces will lead to different DG methods [2]. In our scheme, the numerical traces $\widehat{u}_h$ and $\widehat{q}_h$ are defined in the following way. At the interior cell interfaces,

$$\widehat{u}_h = u_h^- - \boldsymbol{i}\,\beta\,[\![q_h]\!], \tag{2.4a}$$

$$\widehat{q}_h = q_h^+ + \boldsymbol{i}\,\alpha\,[\![u_h]\!], \tag{2.4b}$$

where $[\![\varphi]\!] = \varphi^- - \varphi^+$ represents the jump across the interface. In our error analysis, we assume that the penalty parameters β and α are positive constants. Our numerical experiments show that the method is also well-defined for $\alpha = \beta = 0$, which recovers the LDG method with alternating numerical fluxes.

At the two boundary points $\{a, b\}$,

$$\widehat{u}_h(a) = (1-\gamma)u_h(a) + \boldsymbol{i}\frac{\gamma}{\sqrt{f_a}}\,q_h(a) + 2\gamma, \tag{2.5a}$$

$$\widehat{q}_h(a) = \gamma q_h(a) - \boldsymbol{i}(1-\gamma)\sqrt{f_a}\,u_h(a) + 2\boldsymbol{i}\,(1-\gamma)\sqrt{f_a}, \tag{2.5b}$$

$$\widehat{u}_h(b) = (1-\gamma)u_h(b) - \boldsymbol{i}\frac{\gamma}{\sqrt{f_b}}\,q_h(b), \tag{2.5c}$$

$$\widehat{q}_h(b) = \gamma q_h(b) + \boldsymbol{i}(1-\gamma)\sqrt{f_b}\,u_h(b), \tag{2.5d}$$

where γ can be any real constant in $(0, 1)$. The numerical traces at the boundary are defined in this way to match the boundary conditions in (2.2b). It is easy to see that

$$\widehat{q}_h(a) + \boldsymbol{i}\sqrt{f_a}\,\widehat{u}_h(a) = 2\boldsymbol{i}\sqrt{f_a}, \quad \widehat{q}_h(b) - \boldsymbol{i}\sqrt{f_a}\,\widehat{u}_h(a) = 0.$$

2.3 The multiscale approximation space

For the Schrödinger equation (1.2), WKB asymptotic [6] states that if $E + qV > 0$, when $\hbar \to 0$,

$$\varphi(x) \sim \frac{A}{\sqrt[4]{2m(E+qV(x))}} e^{\boldsymbol{i}S(x)} + \frac{B}{\sqrt[4]{2m(E+qV(x))}} e^{-\boldsymbol{i}S(x)}, \tag{2.6}$$

where A and B are constants and $S(x) = \dfrac{\sqrt{2m}}{\hbar}\displaystyle\int_{x_0}^{x} \sqrt{E+qV(s)}ds$ with integration constant x_0. Therefore, in [5], Ben Abdallah and Pinaud developed

a continuous finite element method using WKB-interpolated basis function

$$\widetilde{\varphi}(x) = \frac{A_j}{\sqrt[4]{2m(E+qV(x))}} e^{\boldsymbol{i}S(x)} + \frac{B_j}{\sqrt[4]{2m(E+qV(x))}} e^{-\boldsymbol{i}S(x)}, \quad x \in I_j.$$

The constants A_j and B_j are determined by the nodal values at the cell boundaries.

Later, Wang and Shu in [18] developed a WKB LDG method using the "constant form" of WKB basis functions. Their finite element space is defined as

$$E^2 = \{v_h : (v_h)|_{I_j} \in \text{span}\{1, e^{\boldsymbol{i}\frac{\sqrt{f(x_j)}}{\varepsilon}(x-x_j)}, e^{-\boldsymbol{i}\frac{\sqrt{f(x_j)}}{\varepsilon}(x-x_j)}\}, \quad j = 1, \ldots, N\},$$

where $\dfrac{\sqrt{f(x_j)}}{\varepsilon} = \dfrac{\sqrt{2m}}{\hbar}\sqrt{E+qV(x_j)}$.

In our new proposed multiscale DG method, we use a more compact approximation space by eliminating 1 in the previous E^2 space. The new finite element space in this paper is defined as

$$E^1 = \{v_h : (v_h)|_{I_j} \in \text{span}\{e^{\boldsymbol{i}\frac{\sqrt{f(x_j)}}{\varepsilon}(x-x_j)}, e^{-\boldsymbol{i}\frac{\sqrt{f(x_j)}}{\varepsilon}(x-x_j)}\}, \quad j = 1, \ldots, N\}.$$

Therefore, our new proposed multiscale DG method is the DG formulation (2.3) in the multiscale finite element space E^1 with numerical traces defined in (2.4) and (2.5).

Remark 1. WKB asymptotic (2.6) is valid only for $E+qV > 0$ and will break down close to turning points which are the points x_j satisfying $E+qV(x_j) = 0$.

Numerically, we require that $f(x_j)$ is not zero so that the basis functions are linearly independent. In implementation, we define a threshold $\tau > 0$. When $|f(x)| < \tau$, we simply replace it by τ in the basis functions. Our numerical tests show that the proposed DG method works for any smooth $f \in W^{1,\infty}([a,b])$.

In our analysis, we assume that $f \in W^{1,\infty}(\Omega)$ and

$$f(x) \geq \tau > 0 \quad \text{for any } x \in \Omega_h. \tag{2.7}$$

When f is negative, the solution is non-oscillatory and the analysis is easier.

3 Error estimates

In this section, we show error estimates of our multiscale DG method for the model problem (2.1).

First, let us introduce the following L^2 projection $\mathbf{\Pi}$. For any $\omega \in H^1(I_j)$ where $I_j \in \Omega_h$, $\mathbf{\Pi}\omega$ is a function in $E^1|_{I_j}$ which satisfies

$$(\omega - \mathbf{\Pi}\omega, \varphi_1)_{I_j} = 0, \tag{3.1a}$$

$$(\omega - \mathbf{\Pi}\omega, \varphi_2)_{I_j} = 0, \tag{3.1b}$$

where

$$\varphi_1 = e^{\boldsymbol{i}\frac{\sqrt{f_j}}{\varepsilon}(x-x_j)} \quad \text{and} \quad \varphi_2 = e^{-\boldsymbol{i}\frac{\sqrt{f_j}}{\varepsilon}(x-x_j)}, \tag{3.2}$$

where $f_j = f(x_j)$.

In the rest of the paper, we use the notation $\delta_\omega = \omega - \mathbf{\Pi}\omega$. The $H^s(D)$-norm is denoted by $\|\cdot\|_{s,D}$. We drop the first subindex if $s = 0$, and the second if $D = \Omega$ or Ω_h. The $L^\infty(\Omega_h)$-norm and the $W^{1,\infty}(\Omega_h)$ semi-norm are denoted as $\|\cdot\|_\infty$ and $|\cdot|_{1,\infty}$, respectively. By default, $(\varphi, v) = (\varphi, v)_{\Omega_h}$ and $\langle \varphi, v\,\boldsymbol{n}\rangle = \langle \varphi, v\,\boldsymbol{n}\rangle_{\partial\Omega_h}$.

We show that the projection $\mathbf{\Pi}$ has the following approximation properties.

Theorem 3.1. *If a function φ is the solution to the equation*

$$-\varepsilon^2\varphi'' - f\varphi = \theta, \tag{3.3}$$

where $\theta \in L^2(\Omega_h)$ and f satisfies (2.7), and $\psi = \varepsilon\varphi'$, then on each $I_j \in \Omega_h$ we have

$$\|\delta_\varphi\|_{I_j} + \|\delta_\psi\|_{I_j} \le C\,\frac{h}{\varepsilon}(\|\theta\|_{I_j} + h|f|_{W^{1,\infty}(I_j)}\|\varphi\|_{I_j})$$

and

$$\|\delta_\varphi\|_{\partial I_j} + \|\delta_\psi\|_{\partial I_j} \le C\,\frac{h^{1/2}}{\varepsilon}(\|\theta\|_{I_j} + h|f|_{W^{1,\infty}(I_j)}\|\varphi\|_{I_j}),$$

where C is independent of ε and h.

The proofs of this Theorem and the remaining theorems in this section will be given in the next section.

Remark 2. Note that Theorem 3.1 holds only for functions which satisfy Equation (3.3). For general smooth functions, the approximation result will require that h is much smaller than the parameter ε. In our error analysis,

we apply Theorem 3.1 to the solutions of the model problem (2.1) and its dual problem, and it is crucial for removing the typical mesh constraint $h \lesssim \varepsilon$ for resolving highly oscillating solutions.

Applying Theorem 3.1 to the solution of (2.1), we immediately get the following result.

Lemma 3.2. *For the exact solution u and q to the equation* (2.2a)*, we have*

$$\|\delta_u\| + \|\delta_q\| \leq C \frac{h^2}{\varepsilon} |f|_{W^{1,\infty}(\Omega_h)} \|u\|$$

and

$$\|\delta_u\|_{\partial\Omega_h} + \|\delta_q\|_{\partial\Omega_h} \leq C \frac{h^{3/2}}{\varepsilon} |f|_{W^{1,\infty}(\Omega_h)} \|u\|.$$

where C is independent of ε and h.

Note that when f is constant, Lemma 3.2 implies that $\delta_u = \delta_q = 0$. This is consistent with the fact that the solutions u and q are in the finite element space E^1 if f is constant.

To state our main results, we need the following notation. Let $e_\omega = \omega - \omega_h$ and $\eta_\omega = \mathbf{\Pi}\omega - \omega_h$. Then $e_\omega = \delta_\omega + \eta_\omega$. First we estimate the jumps of η_u and η_q at the cell interfaces.

Theorem 3.3. *Assume that α and β are positive constants and $0 < \gamma < 1$. For any mesh size $h > 0$, we have*

$$\|[\![\eta_u]\!]\|_{\mathscr{E}_h} + \|[\![\eta_q]\!]\|_{\mathscr{E}_h} \leq C|f|_{1,\infty} \frac{h^{3/2}}{\varepsilon} (\|\eta_u\| + \|u\|),$$

where C is independent of ε and h.

For the projection of errors (η_u, η_q) in the interior of the domain, we have the following result.

Theorem 3.4. *Under the assumption of Theorem 3.3, we have*

$$\|\eta_u\| \leq C|f|_{1,\infty} (\frac{h^2}{\varepsilon} + \frac{h^3}{\varepsilon^2}) \|u\|,$$

where C is independent of ε and h.

Using the triangle inequality, Theorem 3.1 and Theorem 3.4, we now have our error estimate for the actual error $e_u = u - u_h$ as follows.

Theorem 3.5. *Let u be the solution of the problem (2.1) and $u_h \in E^1$ be the multiscale DG approximation defined by (2.3)-(2.5). Assume that α and β are positive constants and $0 < \gamma < 1$. For any mesh size $h > 0$, we have*

$$\|u - u_h\| \leq C|f|_{1,\infty}(\frac{h^2}{\varepsilon} + \frac{h^3}{\varepsilon^2})\|u\|,$$

where C is independent of ε and h.

Theorem 3.5 shows that when f is constant, the error of the multiscale DG method is zero. When f is not constant, the method has a second order convergence rate, and the estimate holds even if $h \gtrsim \varepsilon$.

4 Proofs

In the section, we first prove the projection results in Theorem 3.1, which allow us to carry out error analysis without assuming that h is smaller than ε. Then we use an energy argument to get the error estimate at cell interfaces in Theorem 3.3. Finally, we apply a duality argument to get the main result in Theorem 3.4. Let us begin by introducing some preliminaries.

4.1 Preliminaries

Note that the exact solution to Equation (2.1) also satisfies the weak formulation (2.3). Using the orthogonality property of the projection $\mathbf{\Pi}$ in (3.1), We get the following *error equations*

$$(\eta_q, w) + (\varepsilon\eta_u, w') - \langle \varepsilon\widehat{e}_u, w\,\boldsymbol{n}\rangle = 0 \tag{4.1a}$$

$$(\varepsilon\eta_q, v') - \langle \varepsilon\widehat{e}_q, v\,\boldsymbol{n}\rangle - (f(x)\delta_u, v) - (f(x)\eta_u, v) = 0, \tag{4.1b}$$

for all test functions $v, w \in E^1$, where $\widehat{e}_u = u - \widehat{u}_h$ and $\widehat{e}_q = q - \widehat{q}_h$.

Before we prove our error estimates, let us gather some properties of the numerical traces. It is easy to check that the following two Lemmas hold for the numerical traces defined in (2.4) and (2.5).

Lemma 4.1. *For the numerical traces defined in (2.4) at the interior cell interfaces, we have*

$$\widehat{e}_u = (\delta_u + \eta_u)^- - \boldsymbol{i}\beta([\![\delta_q]\!] + [\![\eta_q]\!]),$$
$$\widehat{e}_q = (\delta_q + \eta_q)^+ + \boldsymbol{i}\alpha([\![\delta_u]\!] + [\![\eta_u]\!]).$$

Lemma 4.2. *For the numerical traces defined in* (2.5) *at the boundary points* $\{a, b\}$*, we have*

$$\widehat{e}_u = (1-\gamma)e_u - \boldsymbol{i}\frac{\gamma}{\sqrt{f}}\, e_q\, \boldsymbol{n},$$
$$\widehat{e}_q = \gamma\, e_q + \boldsymbol{i}(1-\gamma)\sqrt{f}\, e_u\, \boldsymbol{n},$$

which implies that

$$\widehat{e}_q - \boldsymbol{i}\sqrt{f}\, \widehat{e}_u\, \boldsymbol{n} = 0,$$

where $\boldsymbol{n}(a) = -1$ *and* $\boldsymbol{n}(b) = 1$*.*

4.2 Proof of Theorem 3.1

To prove the approximation property of the projection $\mathbf{\Pi}$ in Theorem 3.1, first let us show the following inverse inequality.

Lemma 4.3. *For any function* $v \in E^1$ *and* $I_j \in \Omega_h$*, we have*

$$\|v\|_{\partial I_j} \le C h_j^{-1/2} \|v\|_{I_j},$$

where C *is a constant independent of* ε *and* h_j*.*

Proof. Suppose that $v = c_1\varphi_1 + c_2\varphi_2$ on $I_j = (x_{j-\frac{1}{2}}, x_{j+\frac{1}{2}})$, where φ_1 and φ_2 are the basis functions of $E^1|_{I_j}$ defined in (3.2). Then we have

$$\|v\|^2_{\partial I_j} = |v(x_{j-\frac{1}{2}})|^2 + |v(x_{j+\frac{1}{2}})|^2 = \begin{pmatrix} c_1 & c_2 \end{pmatrix} A \begin{pmatrix} \overline{c}_1 \\ \overline{c}_2 \end{pmatrix}$$

and

$$\|v\|^2_{I_j} = \begin{pmatrix} c_1 & c_2 \end{pmatrix} \begin{pmatrix} (\varphi_1,\varphi_1)_{I_j} & (\varphi_1,\varphi_2)_{I_j} \\ (\varphi_2,\varphi_1)_{I_j} & (\varphi_2,\varphi_2)_{I_j} \end{pmatrix} \begin{pmatrix} \overline{c}_1 \\ \overline{c}_2 \end{pmatrix} = \begin{pmatrix} c_1 & c_2 \end{pmatrix} B \begin{pmatrix} \overline{c}_1 \\ \overline{c}_2 \end{pmatrix},$$

where

$$A = 2\begin{pmatrix} 1 & \cos\sigma \\ \cos\sigma & 1 \end{pmatrix} \quad \text{and} \quad B = h_j \begin{pmatrix} 1 & \frac{\sin\sigma}{\sigma} \\ \frac{\sin\sigma}{\sigma} & 1 \end{pmatrix}$$

with $\sigma := \frac{\sqrt{f_j}}{\varepsilon} h_j$. To find a constant $r > 0$ so that $\|v\|^2_{\partial I_j} \le r\|v\|^2_{I_j}$ for any $v \in E^1$, we need to find the largest eigenvalue of the generalized eigenvalue problem

$$A\mathbf{c} = \lambda B\mathbf{c}.$$

This can be written as

$$B^{-1}A\mathbf{c} = \lambda\mathbf{c},$$

so we only need to find the largest eigenvalue of $B^{-1}A$. The two eigenvalues of $B^{-1}A$ are

$$\lambda_1 = 2h_j^{-1}\frac{1+\cos\sigma}{1+\frac{\sin\sigma}{\sigma}} \quad \text{and} \quad \lambda_2 = 2h_j^{-1}\frac{1-\cos\sigma}{1-\frac{\sin\sigma}{\sigma}}.$$

Obviously,

$$|\lambda_1| \le Ch_j^{-1} \quad \text{for any } \sigma > 0.$$

Let us estimate λ_2. If $h_j > c_0\frac{\varepsilon}{\sqrt{f_j}}$ for some $c_0 \in (0, \frac{1}{2}]$, then $\sigma > c_0$. We get

$$\frac{\sin\sigma}{\sigma} < \frac{\sin c_0}{c_0} < 1 \quad \text{and} \quad \frac{1}{1-\frac{\sin\sigma}{\sigma}} < \frac{1}{1-\frac{\sin c_0}{c_0}},$$

which implies that

$$|\lambda_2| \le Ch_j^{-1}.$$

If $h_j < \frac{1}{2}\frac{\varepsilon}{\sqrt{f_j}}$ on I_j, then $0 < \sigma < \frac{1}{2}$. We get $\frac{1-\cos\sigma}{1-\frac{\sin\sigma}{\sigma}} \le C$, and then $|\lambda_2| \le Ch_j^{-1}$. So we have

$$\max\{|\lambda_1|, |\lambda_2|\} \le Ch_j^{-1},$$

which implies

$$\|v\|^2_{\partial I_j} \le Ch_j^{-1}\|v\|^2_{I_j}.$$

□

Next, let us prove Theorem 3.1 by using Lemma 4.3 in four steps.

Proof. It is easy to check that

$$-\varepsilon^2(\mathbf{\Pi}\varphi)'' - f_j\,\mathbf{\Pi}\varphi = 0 \quad \text{on each } I_j,\ j = 1, \cdots, N.$$

Let $\delta_\varphi = \varphi - \mathbf{\Pi}\varphi$. Then δ_φ satisfies the equation

$$-\varepsilon^2\delta_\varphi'' - f_j\delta_\varphi = \theta + (f - f_j)\varphi,$$

which is equivalent to

$$\delta_\varphi'' + \frac{f_j}{\varepsilon^2}\delta_\varphi = g(x), \tag{4.2}$$

where $g(x) = -(\theta + (f - f_j)\varphi)/\varepsilon^2$. So we can assume

$$\delta_\varphi = c_1\varphi_1 + c_2\varphi_2 + Y(x),$$

where φ_1 and φ_2 are the basis functions of $E^1|_{I_j}$ defined in (3.2), and $Y(x)$ is a particular solution to (4.2).

(i) Let us compute and estimate $Y(x)$. Since φ_1 and φ_2 are two solutions to the homogeneous equation corresponding to (4.2), we use variation of parameters and get

$$Y = v_1(x)\varphi_1(x) + v_2(x)\varphi_2(x),$$

where

$$v_1(x) = -\frac{\boldsymbol{i}\varepsilon}{2\sqrt{f_j}}\int_{x_j}^{x} \varphi_2 g\, dx, \quad \text{and} \quad v_2(x) = \frac{\boldsymbol{i}\varepsilon}{2\sqrt{f_j}}\int_{x_j}^{x} \varphi_1 g\, dx.$$

It is easy to see that for any $x \in I_j \cup \partial I_j$,

$$|v_i(x)| \leq C\varepsilon \int_{x_j}^{x} |g| dx \leq \frac{C}{\varepsilon}(h^{1/2}\|\theta\|_{I_j} + h^{3/2}|f|_{W^{1,\infty}(I_j)}\|\varphi\|_{I_j}), \quad i = 1, 2. \tag{4.3}$$

Therefore,

$$\|Y\|_{I_j} \leq \frac{C}{\varepsilon}(h\|\theta\|_{I_j} + h^2|f|_{W^{1,\infty}(I_j)}\|\varphi\|_{I_j}). \tag{4.4}$$

(ii) Let us compute and estimate the term $c_1\varphi_1 + c_2\varphi_2$ in δ_φ. By the definition of the projection $\mathbf{\Pi}$, (3.1), we have

$$(\delta_\varphi, \varphi_1)_{I_j} = 0, \quad (\delta_\varphi, \varphi_2)_{I_j} = 0.$$

After some calculations, we can write the above linear system as

$$h_j \begin{pmatrix} 1 & \frac{\sin\sigma}{\sigma} \\ \frac{\sin\sigma}{\sigma} & 1 \end{pmatrix} \begin{pmatrix} c_1 \\ c_2 \end{pmatrix} = - \begin{pmatrix} (Y, \varphi_1)_{I_j} \\ (Y, \varphi_2)_{I_j} \end{pmatrix}.$$

The solution to the linear system is

$$c_1 = D_1 D_2 \quad \text{and} \quad c_2 = D_1 D_3,$$

where

$$\begin{aligned} D_1 =& - h_j^{-1}(1 - \frac{\sin^2\sigma}{\sigma^2})^{-1}, \\ D_2 =& (Y, \varphi_1 - \frac{\sin\sigma}{\sigma}\varphi_2)_{I_j}, \\ D_3 =& (Y, \varphi_2 - \frac{\sin\sigma}{\sigma}\varphi_1)_{I_j}. \end{aligned}$$

Note that

$$c_1\varphi_1 + c_2\varphi_2 = D_1\big((D_2 + D_3)\cos\frac{\sqrt{f_j}}{\varepsilon}(x - x_j) + \boldsymbol{i}(D_2 - D_3)\sin\frac{\sqrt{f_j}}{\varepsilon}(x - x_j)\big).$$

Because

$$D_2 + D_3 = 2(1 - \frac{\sin\sigma}{\sigma})(Y, \cos\frac{\sqrt{f_j}}{\varepsilon}(x - x_j))_{I_j}$$

and

$$D_2 - D_3 = 2(1 + \frac{\sin\sigma}{\sigma})(Y, \boldsymbol{i}\,\sin\frac{\sqrt{f_j}}{\varepsilon}(x - x_j))_{I_j},$$

we have

$$\begin{aligned} \|c_1\varphi_1 + c_2\varphi_2\|_{I_j} \leq & 2|D_1|(1 - \frac{\sin\sigma}{\sigma})\|Y\|_{I_j}\|\cos\frac{\sqrt{f_j}}{\varepsilon}(x - x_j)\|_{I_j}^2 \\ & + 2|D_1|(1 + \frac{\sin\sigma}{\sigma})\|Y\|_{I_j}\|\sin\frac{\sqrt{f_j}}{\varepsilon}(x - x_j)\|_{I_j}^2. \end{aligned}$$

It is easy to check that

$$\|\sin\frac{\sqrt{f_j}}{\varepsilon}(x - x_j)\|_{I_j}^2 = \frac{1}{2}h(1 - \frac{\sin\sigma}{\sigma})$$

and

$$\|\cos\frac{\sqrt{f_j}}{\varepsilon}(x - x_j)\|_{I_j}^2 = \frac{1}{2}h(1 + \frac{\sin\sigma}{\sigma}).$$

So we have

$$\|c_1\varphi_1 + c_2\varphi_2\|_{I_j} \leq 2\|Y\|_{I_j} \leq C\,\frac{h}{\varepsilon}(\|\theta\|_{I_j} + h|f|_{W^{1,\infty}}\|\varphi\|_{I_j}). \qquad (4.5)$$

(*iii*) Now we estimate $\|\delta_\varphi\|_{I_j}$ and $\|\delta_\psi\|_{I_j}$. From (4.4) and (4.5), we immediately get

$$\|\delta_\varphi\|_{I_j} \le 3\|Y\|_{I_j} \le C\,\frac{h}{\varepsilon}(\|\theta\|_{I_j} + h|f|_{W^{1,\infty}}\|\varphi\|_{I_j}).$$

To estimate δ_ψ, we let

$$v_\psi = \varepsilon(\mathbf{\Pi}\varphi)' - 2\boldsymbol{i}\sqrt{f_j}\,c_2\varphi_2.$$

Since $v_\psi \in E^1$, we have

$$\|\delta_\psi\|_{I_j} \le \|\psi - v_\psi\|_{I_j}.$$

So we only need to estimate $\psi - v_\psi$. Note that

$$\psi - v_\psi = \varepsilon\delta'_\varphi + 2\boldsymbol{i}\sqrt{f_j}\,c_2\,\varphi_2 = \boldsymbol{i}\sqrt{f_j}(c_1\varphi_1 + c_2\varphi_2) + \varepsilon Y'. \tag{4.6}$$

Hence,

$$\|\psi - v_\psi\|_{I_j} \le \sqrt{f_j}\|c_1\varphi_1 + c_2\varphi_2\|_{I_j} + \|\varepsilon Y'\|_{I_j}.$$

It is easy to check that

$$Y' = v_1'\varphi_1 + v_1\varphi_1' + v_2'\varphi_2 + v_2\varphi_2' = v_1\varphi_1' + v_2\varphi_2'. \tag{4.7}$$

So

$$\begin{aligned}\|\varepsilon Y'\|_{I_j} \le& \|v_1\|_{L^\infty(I_j)}\|\varepsilon\varphi_1'\|_{I_j} + \|v_2\|_{L^\infty(I_j)}\|\varepsilon\varphi_2'\|_{I_j}\\ \le& Ch_j^{1/2}(\|v_1\|_{L^\infty(I_j)} + \|v_2\|_{L^\infty(I_j)}).\end{aligned}$$

Using (4.3), we have

$$\|\varepsilon Y'\|_{I_j} \le C\frac{h}{\varepsilon}(\|\theta\|_{I_j} + h|f|_{W^{1,\infty}(I_j)}\|\varphi\|_{I_j}).$$

Using the inequality above and (4.5), we get

$$\|\delta_\psi\|_{I_j} \le \|\psi - v_\psi\|_{I_j} \le C\frac{h}{\varepsilon}(\|\theta\|_{I_j} + h|f|_{W^{1,\infty}(I_j)}\|\varphi\|_{I_j}). \tag{4.8}$$

(*iv*) Let us estimate $\|\delta_\varphi\|_{\partial I_j}$ and $\|\delta_\psi\|_{\partial I_j}$. Because $\delta_\varphi = c_1\varphi_1 + c_2\varphi + Y$ and $c_1\varphi_1 + c_2\varphi_2 \in E^1$, by Lemma 4.3 we have

$$\|\delta_\varphi\|_{\partial I_j} \le Ch^{-1/2}\|c_1\varphi_1 + c_2\varphi_2\|_{I_j} + \|Y\|_{\partial I_j}.$$

Using the triangle inequality and (4.3), we get

$$\begin{aligned}\|Y\|_{\partial I_j} \leq & \|v_1\|_{L^\infty(\partial I_j)}\|\varphi_1\|_{\partial I_j} + \|v_2\|_{L^\infty(\partial I_j)}\|\varphi_2\|_{\partial I_j} \\ \leq & \|v_1\|_{L^\infty(\partial I_j)} + \|v_2\|_{L^\infty(\partial I_j)} \\ \leq & \frac{C}{\varepsilon}(h^{1/2}\|\theta\|_{I_j} + h^{3/2}|f|_{W^{1,\infty}(I_j)}\|\varphi\|_{I_j}).\end{aligned}$$

Using the last inequality and (4.5) we have

$$\|\delta_\varphi\|_{\partial I_j} \leq C\frac{h^{1/2}}{\varepsilon}(\|\theta\|_{I_j} + h|f|_{W^{1,\infty}(I_j)}\|\varphi\|_{I_j}).$$

Next, we estimate $\|\delta_\psi\|_{\partial I_j}$. Using the triangle inequality and the expression of $\psi - v_\psi$, (4.6), we get

$$\begin{aligned}\|\delta_\psi\|_{\partial I_j} \leq & \|\psi - v_\psi\|_{\partial I_j} + \|v_\psi - \mathbf{\Pi}\psi\|_{\partial I_j} \\ \leq & C\|c_1\varphi_1 + c_2\varphi_2\|_{\partial I_j} + \|\varepsilon Y'\|_{\partial I_j} + \|v_\psi - \mathbf{\Pi}\psi\|_{\partial I_j}.\end{aligned}$$

Note that $c_1\varphi_1 + c_2\varphi_2 \in E^1$ and $v_\psi - \mathbf{\Pi}\psi \in E^1$. By Lemma 4.3, we get

$$\|\delta_\psi\|_{\partial I_j} \leq Ch^{-1/2}(\|c_1\varphi_1 + c_2\varphi_2\|_{I_j} + \|v_\psi - \mathbf{\Pi}\psi\|_{I_j}) + \|\varepsilon Y'\|_{\partial I_j}. \tag{4.9}$$

From the equation (4.7), we obtain that

$$\begin{aligned}\|\varepsilon Y'\|_{\partial I_j} \leq & \|v_1\|_{L^\infty(\partial I_j)}\|\varepsilon\varphi_1'\|_{\partial I_j} + \|v_2\|_{L^\infty(\partial I_j)}\|\varepsilon\varphi_2'\|_{\partial I_j} \\ \leq & C(\|v_1\|_{L^\infty(\partial I_j)} + \|v_2\|_{L^\infty(\partial I_j)}).\end{aligned}$$

Then by (4.3), we have

$$\|\varepsilon Y'\|_{\partial I_j} \leq C\,\frac{h^{1/2}}{\varepsilon}(\|\theta\|_{I_j} + h|f|_{W^{1,\infty}(I_j)}\|\varphi\|_{I_j}). \tag{4.10}$$

Note that

$$\|v_\psi - \mathbf{\Pi}\psi\|_{I_j} \leq \|v_\psi - \psi\|_{I_j} + \|\psi - \mathbf{\Pi}\psi\|_{I_j} \leq 2\|v_\psi - \psi\|_{I_j}.$$

Using (4.8), we get

$$\|v_\psi - \mathbf{\Pi}\psi\|_{I_j} \leq C\frac{h}{\varepsilon}\,(\|\theta\|_{I_j} + h|f|_{W^{1,\infty}(I_j)}\|\varphi\|_{I_j}). \tag{4.11}$$

Applying (4.10), (4.11) and (4.5) to (4.9), we get

$$\|\delta_\psi\|_{\partial I_j} \leq C\frac{h^{1/2}}{\varepsilon}(\|\theta\|_{I_j} + h|f|_{W^{1,\infty}(I_j)}\|\varphi\|_{I_j}).$$

□

4.3 Proof of Theorem 3.3

To prove Theorem 3.3, first we show the following Lemma by an energy argument.

Lemma 4.4.

$$L = B_1 + B_2,$$

where

$$\begin{aligned}
L =&\|\eta_q\|^2 - (f, |\eta_u|^2) + \boldsymbol{i}\beta\varepsilon\|[\![\eta_q]\!]\|^2_{\mathscr{E}_h^i} + \boldsymbol{i}\alpha\varepsilon\|[\![\eta_u]\!]\|^2_{\mathscr{E}_h^i} \\
&+ \boldsymbol{i}\gamma\varepsilon\langle\frac{1}{\sqrt{f}}, |\eta_q|^2\rangle_{\partial\Omega} + \boldsymbol{i}(1-\gamma)\varepsilon\langle|\eta_u|^2, \sqrt{f}\rangle_{\partial\Omega}, \\
B_1 =&(\eta_u, f\delta_u), \\
B_2 =&\varepsilon\,\langle\delta_u^-,\, \eta_q\,\boldsymbol{n}\rangle_{\partial\Omega_h\setminus\partial\Omega} + \varepsilon\,\langle\eta_u,\, \delta_q^+\,\boldsymbol{n}\rangle_{\partial\Omega_h\setminus\partial\Omega} \\
&- \boldsymbol{i}\alpha\varepsilon\,\langle\eta_u,\, [\![\delta_u]\!]\,\boldsymbol{n}\rangle_{\partial\Omega_h\setminus\partial\Omega} - \boldsymbol{i}\beta\varepsilon\,\langle[\![\delta_q]\!],\, \eta_q\,\boldsymbol{n}\rangle_{\partial\Omega_h\setminus\partial\Omega} \\
&+ \varepsilon\,\langle(1-\gamma)\delta_u - \boldsymbol{i}\frac{\gamma}{\sqrt{f}}\delta_q\,\boldsymbol{n},\, \eta_q\,\boldsymbol{n}\rangle_{\partial\Omega} + \varepsilon\,\langle\eta_u,\, \gamma\delta_q\,\boldsymbol{n} + \boldsymbol{i}(1-\gamma)\sqrt{f}\delta_u\rangle_{\partial\Omega}.
\end{aligned}$$

Proof. Taking $w = \eta_q$ in the error equation (4.1a) and $v = \eta_u$ in the complex conjugate of (4.1b) and adding the equations together, we get

$$\begin{aligned}
0 =&(\eta_q, \eta_q) + \varepsilon(\eta_u, \eta_q') - \varepsilon\langle\widehat{e}_u, \eta_q\,\boldsymbol{n}\rangle \\
&+ \varepsilon(\eta_u', \eta_q) - \varepsilon\langle\eta_u, \widehat{e}_q\,\boldsymbol{n}\rangle - (\eta_u, f\,\eta_u) - (\eta_u, f\,\delta_u).
\end{aligned}$$

Using integration by parts for the second term on the right hand side of the equation, we have

$$0 = \|\eta_q\|^2 - (\eta_u, f\,\eta_u) - (\eta_u, f\,\delta_u) + \Theta, \tag{4.12}$$

where

$$\Theta = \varepsilon\langle\eta_u, \eta_q\,\boldsymbol{n}\rangle - \varepsilon\langle\widehat{e}_u, \eta_q\,\boldsymbol{n}\rangle - \varepsilon\langle\eta_u, \widehat{e}_q\,\boldsymbol{n}\rangle.$$

Using Lemma 4.1 to rewrite $\widehat{e}_u$ and $\widehat{e}_q$ on interior cell interfaces, we get

$$\Theta = \sum_{k=1}^{4} A_k$$

where

$$
\begin{aligned}
A_1 =&\varepsilon\langle\eta_u, \eta_q\,\boldsymbol{n}\rangle_{\partial\Omega_h\setminus\partial\Omega} - \varepsilon\langle\eta_u^-, \eta_q\,\boldsymbol{n}\rangle_{\partial\Omega_h\setminus\partial\Omega} - \varepsilon\langle\eta_u, \eta_q^+\,\boldsymbol{n}\rangle_{\partial\Omega_h\setminus\partial\Omega},\\
A_2 =&-\varepsilon\langle\delta_u^-, \eta_q\,\boldsymbol{n}\rangle_{\partial\Omega_h\setminus\partial\Omega} - \varepsilon\langle\eta_u, \delta_q^+\,\boldsymbol{n}\rangle_{\partial\Omega_h\setminus\partial\Omega},\\
A_3 =&\boldsymbol{i}\beta\varepsilon\langle[\![\delta_q]\!] + [\![\eta_q]\!], \eta_q\,\boldsymbol{n}\rangle_{\partial\Omega_h\setminus\partial\Omega} + \boldsymbol{i}\alpha\varepsilon\langle\eta_u, ([\![\delta_u]\!] + [\![\eta_u]\!])\boldsymbol{n}\rangle_{\partial\Omega_h\setminus\partial\Omega},\\
A_4 =&\varepsilon\langle\eta_u, \eta_q\,\boldsymbol{n}\rangle_{\partial\Omega} - \varepsilon\langle\widehat{e}_u, \eta_q\,\boldsymbol{n}\rangle_{\partial\Omega} - \varepsilon\langle\eta_u, \widehat{e}_q\,\boldsymbol{n}\rangle_{\partial\Omega}.
\end{aligned}
$$

It is easy to see that

$$A_1 = 0,$$

and

$$A_3 = \boldsymbol{i}\beta\varepsilon\|[\![\eta_q]\!]\|^2_{\mathscr{E}_h^i} + \boldsymbol{i}\alpha\varepsilon\|[\![\eta_u]\!]\|^2_{\mathscr{E}_h^i} + \boldsymbol{i}\beta\varepsilon\langle[\![\delta_q]\!], \eta_q\,\boldsymbol{n}\rangle_{\partial\Omega_h\setminus\partial\Omega} + \boldsymbol{i}\alpha\varepsilon\langle\eta_u, [\![\delta_u]\!]\,\boldsymbol{n}\rangle_{\partial\Omega_h\setminus\partial\Omega}.$$

Using Lemma 4.2 and the fact that $e_\omega = \delta_\omega + \eta_\omega$ for $\omega = u, q$ to rewrite $\widehat{e}_u$ and $\widehat{e}_q$ on the domain boundary, we obtain

$$
\begin{aligned}
A_4 =&\boldsymbol{i}\gamma\varepsilon\,\langle\frac{1}{\sqrt{f}}\eta_q, \eta_q\rangle_{\partial\Omega} + \boldsymbol{i}(1-\gamma)\varepsilon\,\langle\eta_u, \sqrt{f}\eta_u\rangle_{\partial\Omega}\\
&-\varepsilon\,\langle(1-\gamma)\delta_u - \boldsymbol{i}\frac{\gamma}{\sqrt{f}}\delta_q\,\boldsymbol{n}, \eta_q\,\boldsymbol{n}\rangle_{\partial\Omega} - \varepsilon\,\langle\eta_u, \gamma\delta_q\,\boldsymbol{n} + \boldsymbol{i}(1-\gamma)\sqrt{f}\delta_u\rangle_{\partial\Omega}.
\end{aligned}
$$

Adding above expressions of A_1, A_2, A_3, A_4 to get Θ and using it in (4.12), we get the conclusion. □

Now let us prove Theorem 3.3 using Lemma 4.4 and Lemma 3.2.

Proof. Taking the imaginary part of L in Lemma 4.4, we get

$$\beta\varepsilon\|[\![\eta_q]\!]\|^2_{\mathscr{E}_h^i} + \alpha\varepsilon\|[\![\eta_u]\!]\|^2_{\mathscr{E}_h^i} + \gamma\varepsilon\langle\frac{1}{\sqrt{f}}, |\eta_q|^2\rangle_{\partial\Omega} + (1-\gamma)\varepsilon\langle|\eta_u|^2, \sqrt{f}\rangle_{\partial\Omega} \le |B_1| + |B_2|.$$

Now we estimate B_1 and B_2. Let $\mathbb{P}^0$ be the L^2 projection onto constant functions on each element $I_j \in \Omega_h$. Using the orthogonality property of the projection $\boldsymbol{\Pi}$, we have

$$|B_1| = |\big(\eta_u, (f - \mathbb{P}^0 f)\delta_u\big)| \le Ch|f|_{1,\infty}\|\delta u\|\|\eta_u\|.$$

Using the Cauchy inequality, we get

$$\begin{aligned}|B_2| \leq & C\varepsilon \|[\![\eta_q]\!]\|_{\mathscr{E}_h^i}(\|\delta_u\|_{\partial\Omega_h\setminus\partial\Omega} + \beta\|\delta_q\|_{\partial\Omega_h\setminus\partial\Omega}) \\ & + C\varepsilon \|[\![\eta_u]\!]\|_{\mathscr{E}_h^i}(\|\delta_q\|_{\partial\Omega_h\setminus\partial\Omega} + \alpha\|\delta_u\|_{\partial\Omega_h\setminus\partial\Omega}) \\ & + C\varepsilon \|\eta_q\|_{\partial\Omega}\Big((1-\gamma)\|\delta_u\|_{\partial\Omega} + \gamma\|\delta_q\|_{\partial\Omega}\Big) \\ & + C\varepsilon \|\eta_u\|_{\partial\Omega}\Big(\gamma\|\delta_q\|_{\partial\Omega} + (1-\gamma)\|\delta_u\|_{\partial\Omega}\Big)\end{aligned}$$

Because α, β are positive constant and $0 < \gamma < 1$, we have

$$|B_2| \leq C\varepsilon(\|[\![\eta_q]\!]\|_{\mathscr{E}_h} + \|[\![\eta_u]\!]\|_{\mathscr{E}_h})(\|\delta_u\|_{\partial\Omega_h} + \|\delta_q\|_{\partial\Omega_h}).$$

So

$$\begin{aligned}&\beta\|[\![\eta_q]\!]\|^2_{\mathscr{E}_h^i} + \alpha\|[\![\eta_u]\!]\|^2_{\mathscr{E}_h^i} + \gamma\langle\frac{1}{\sqrt{f}}, |\eta_q|^2\rangle_{\partial\Omega} + (1-\gamma)\langle\sqrt{f}, |\eta_u|^2\rangle_{\partial\Omega} \\ \leq & \frac{1}{\varepsilon}(|B_1| + |B_2|) \\ \leq & C\frac{h}{\varepsilon}|f|_{1,\infty}\|\delta_u\|\|\eta_u\| + C(\|[\![\eta_q]\!]\|_{\mathscr{E}_h} + \|[\![\eta_u]\!]\|_{\mathscr{E}_h})(\|\delta_u\|_{\partial\Omega_h} + \|\delta_q\|_{\partial\Omega_h}),\end{aligned}$$

which implies that

$$\begin{aligned}\|[\![\eta_q]\!]\|^2_{\mathscr{E}_h} + \|[\![\eta_u]\!]\|^2_{\mathscr{E}_h} \leq & C\frac{h}{\varepsilon}|f|_{1,\infty}\|\delta_u\|\|\eta_u\| + C(\|\delta_u\|^2_{\partial\Omega_h} + \|\delta_q\|^2_{\partial\Omega_h}) \\ \leq & C\frac{h^3}{\varepsilon^2}|f|^2_{1,\infty}\|\eta_u\|^2 + \frac{C}{h}\|\delta_u\|^2 + C(\|\delta_u\|^2_{\partial\Omega_h} + \|\delta_q\|^2_{\partial\Omega_h}).\end{aligned}$$

Finally, applying the projection result in Lemma 3.2, we get

$$\|[\![\eta_q]\!]\|^2_{\mathscr{E}_h} + \|[\![\eta_u]\!]\|^2_{\mathscr{E}_h} \leq C\frac{h^3}{\varepsilon^2}|f|^2_{1,\infty}(\|\eta_u\|^2 + \|u\|^2),$$

which completes the proof. □

4.4 Proof of Theorem 3.4

To obtain the error estimates for u_h in Theorem 3.4, we use a duality argument. We first consider the following dual problem for any given $\theta \in$

$L^2(\Omega)$

$$\psi - \varepsilon\varphi' = 0 \quad \text{in } \Omega, \tag{4.13a}$$
$$-\varepsilon\psi' - f\varphi = \theta \quad \text{in } \Omega, \tag{4.13b}$$
$$\psi(a) - \boldsymbol{i}\sqrt{f}_a\,\varphi(a) = 0, \tag{4.13c}$$
$$\psi(b) + \boldsymbol{i}\sqrt{f}_b\,\varphi(b) = 0. \tag{4.13d}$$

For the dual problem, we have the following regularity result.

Lemma 4.5. *Given $\theta \in L^2(\Omega)$, the solution φ and ψ of the dual problem* (4.13) *satisfy*

$$\|\psi\| + \|\varphi\| \le C\varepsilon^{-1}\|\theta\|,$$

where C is independent of ε.

Proof. From (4.13a) and (4.13b) we get

$$-\varepsilon^2\varphi'' - f\varphi = \theta. \tag{4.14}$$

First, we multiply the equation (4.14) by $\overline{\varphi}$ and integrate over Ω to get

$$-\varepsilon^2(\varphi'', \varphi)_\Omega - (f, |\varphi|^2)_\Omega = (\theta, \varphi)_\Omega.$$

Using integration by parts and the boundary conditions (4.13c) and (4.13d), we get

$$\|\varepsilon\varphi'\|^2 - (f, |\varphi|^2)_\Omega + \boldsymbol{i}\varepsilon\sqrt{f_b}\,|\varphi(b)|^2 + \boldsymbol{i}\varepsilon\sqrt{f_a}\,|\varphi(a)|^2 = (\theta, \varphi)_\Omega.$$

Taking the imaginary part of above equation, we get

$$|\varphi(b)|^2 + |\varphi(a)|^2 \le C\varepsilon^{-1}\|\theta\|\|\varphi\| \tag{4.15}$$

which implies that

$$|\varepsilon\varphi'(b)|^2 + |\varepsilon\varphi'(a)|^2 \le C\varepsilon^{-1}\|\theta\|\|\varphi\| \tag{4.16}$$

by using the boundary conditions (4.13c) and (4.13d).

Next, we multiply the equation (4.14) by $\overline{\varphi}'$ and get

$$-\varepsilon^2\varphi''\overline{\varphi}' - f\varphi\overline{\varphi}' = \theta\overline{\varphi}'.$$

Taking the real part of the above equation, we have

$$-\frac{1}{2}\frac{d}{dx}|\varepsilon\varphi'|^2-\frac{1}{2}\frac{d}{dx}(f|\varphi|^2)=-\frac{1}{2}f'|\varphi|^2+\mathrm{Re}(\theta\overline{\varphi}'),$$

which implies

$$\begin{aligned}\frac{d}{dx}(|\varepsilon\varphi'|^2+f|\varphi|^2)=&f'|\varphi|^2-2\mathrm{Re}(\theta\overline{\varphi}')\\ \le&C|\varphi|^2+|\varepsilon\varphi'|^2+\frac{1}{\varepsilon^2}|\theta|^2\\ \le&C(|\varepsilon\varphi'|^2+f|\varphi|^2)+\frac{1}{\varepsilon^2}|\theta|^2.\end{aligned}$$

Let $G(x)=|\varepsilon\varphi'|^2+f|\varphi|^2$. Then from above we have

$$G'(x)\le CG(x)+\frac{1}{\varepsilon^2}|\theta(x)|^2.$$

Using Gronwall's inequality, we get

$$G(x)\le CG(a)+C\int_a^x\frac{1}{\varepsilon^2}|\theta(x)|^2dx\le C(G(a)+\frac{1}{\varepsilon^2}\|\theta\|^2).$$

From (4.15) and (4.16), we have

$$G(a)=|\varepsilon\varphi'(a)|^2+f(a)|\varphi(a)|^2\le C\frac{1}{\varepsilon}\|\theta\|\|\varphi\|.$$

So

$$G(x)\le C\frac{1}{\varepsilon}\|\theta\|\|\varphi\|+\frac{1}{\varepsilon^2}\|\theta\|^2.$$

Now integrating $G(x)$ over $[a,b]$, we obtain

$$\|\varepsilon\varphi'\|^2+\tau\|\varphi\|^2\le\int_a^bG(x)dx\le C\frac{1}{\varepsilon}\|\theta\|\|\varphi\|+C\frac{1}{\varepsilon^2}\|\theta\|^2\le C\frac{1}{\varepsilon^2}\|\theta\|^2+\frac{\tau}{2}\|\varphi\|^2.$$

Therefore,

$$\|\varepsilon\varphi'\|^2+\|\varphi\|^2\le C\frac{1}{\varepsilon^2}\|\theta\|^2.$$

□

Using the projection result in Theorem 3.1 and the regularity result in Lemma 4.5, we immediately get the following result.

Lemma 4.6. *For the solution φ and ψ to the dual problem* (4.13)*, we have*

$$\|\delta_\varphi\| + \|\delta_\psi\| \leq C(\frac{h}{\varepsilon} + \frac{h^2}{\varepsilon^2})\|\theta\|$$

and

$$\|\delta_\varphi\|_{\partial\Omega_h} + \|\delta_\psi\|_{\partial\Omega_h} \leq C(\frac{h^{1/2}}{\varepsilon} + \frac{h^{3/2}}{\varepsilon^2})\|\theta\|.$$

We are now ready to prove Theorem 3.4.

Lemma 4.7. *For any $\theta \in L^2(\Omega_h)$, we have*

$$(\eta_u, \theta)_{\Omega_h} = S_1 + S_2,$$

where

$$\begin{aligned} S_1 =& -\varepsilon\langle\eta_u, \delta_\psi \boldsymbol{n}\rangle + \varepsilon\langle\eta_q, \delta_\varphi \boldsymbol{n}\rangle - \varepsilon\langle\widehat{e}_q, \delta_\varphi \boldsymbol{n}\rangle + \varepsilon\langle\widehat{e}_u, \delta\psi \boldsymbol{n}\rangle, \\ S_2 =& ((f - \mathbb{P}^0 f)\eta_u, \delta\varphi) + ((f - \mathbb{P}^0 f)\delta_u, \mathbf{\Pi}\varphi). \end{aligned}$$

Proof. By the equation (4.13b) in the dual problem , we have

$$\begin{aligned} (\eta_u, \theta) =& -(\eta_u, \varepsilon\psi') - (\eta_u, f\varphi) \\ =& -\varepsilon(\eta_u, \delta'_\psi) - \varepsilon(\eta_u, (\mathbf{\Pi}\psi)') - (\eta_u, f\varphi). \end{aligned}$$

Using integration by parts and the property of the projection $\mathbf{\Pi}$ (3.1), we have

$$\begin{aligned} (\eta_u, \theta) =& -\varepsilon\langle\eta_u, \delta_\psi \boldsymbol{n}\rangle + \varepsilon(\eta'_u, \delta_\psi) - \varepsilon(\eta_u, (\mathbf{\Pi}\psi)') - (\eta_u, f\varphi) \\ =& -\varepsilon\langle\eta_u, \delta_\psi \boldsymbol{n}\rangle - \varepsilon(\eta_u, (\mathbf{\Pi}\psi)') - (\eta_u, f\varphi) \end{aligned}$$

Using the error equation (4.1a) with $\omega = \mathbf{\Pi}\psi$, we get

$$(\eta_u, \theta) = -\varepsilon\langle\eta_u, \delta_\psi \boldsymbol{n}\rangle + (\eta_q, \mathbf{\Pi}\psi) - \varepsilon\langle\widehat{e}_u, \mathbf{\Pi}\psi \boldsymbol{n}\rangle - (\eta_u, f\varphi).$$

For the second term on the right hand side of the equation, we use the definition of the projection $\mathbf{\Pi}$ and then the equation (4.13b) to get

$$(\eta_q, \mathbf{\Pi}\psi) = (\eta_q, \psi) = (\eta_q, \varepsilon\varphi') = \varepsilon(\eta_q, \delta'_\varphi) + \varepsilon(\eta_q, (\mathbf{\Pi}\varphi)').$$

Using integration by parts and the definition of the projection $\mathbf{\Pi}$, we have

$$(\eta_q, \mathbf{\Pi}\psi) = \varepsilon\langle\eta_q, \delta_\varphi \boldsymbol{n}\rangle + \varepsilon(\eta_q, (\mathbf{\Pi}\varphi)').$$

For the second term on the right hand side of the equation, we use the error equation (4.1b) with $v = \mathbf{\Pi}\varphi$ and obtain

$$(\eta_q, \mathbf{\Pi}\psi) = \varepsilon\langle \eta_q, \delta_\varphi \boldsymbol{n}\rangle + \varepsilon\langle \widehat{e}_q, \mathbf{\Pi}\varphi \boldsymbol{n}\rangle + (f\eta_u, \mathbf{\Pi}\varphi) + (f\delta_u, \mathbf{\Pi}\varphi).$$

So we have

$$\begin{aligned}(\eta_u, \theta) = &- \varepsilon\langle \eta_u, \delta_\psi \boldsymbol{n}\rangle + \varepsilon\langle \eta_q, \delta_\varphi \boldsymbol{n}\rangle + \varepsilon\langle \widehat{e}_q, \mathbf{\Pi}\varphi \boldsymbol{n}\rangle \\ &- (f\eta_u, \delta\varphi) + (f\delta_u, \mathbf{\Pi}\varphi) - \varepsilon\langle \widehat{e}_u, \mathbf{\Pi}\psi \boldsymbol{n}\rangle.\end{aligned}$$

It is easy to check that $-\langle \widehat{e}_q, \varphi \boldsymbol{n}\rangle + \langle \widehat{e}_u, \psi \boldsymbol{n}\rangle = 0$. So

$$\begin{aligned}(\eta_u, \theta) = &- \varepsilon\langle \eta_u, \delta_\psi \boldsymbol{n}\rangle + \varepsilon\langle \eta_q, \delta_\varphi \boldsymbol{n}\rangle - \varepsilon\langle \widehat{e}_q, \delta_\varphi \boldsymbol{n}\rangle + \varepsilon\langle \widehat{e}_u, \delta\psi \boldsymbol{n}\rangle \\ &- (f\eta_u, \delta\varphi) + (f\delta_u, \mathbf{\Pi}\varphi).\end{aligned}$$

The Lemma follows by using the definition of the L^2 projection $\mathbf{\Pi}$. □

For single-valued functions v and w at $\mathscr{E}_h^i$, let us introduce the notation

$$\langle v, \omega\rangle_{\mathscr{E}_h^i} = \sum_{j=1}^{N-1} v(x_{j+\frac{1}{2}}) w(x_{j+\frac{1}{2}}).$$

Now we prove Theorem 3.4.

Proof. Taking $\theta = \eta_u$, we have

$$\|\eta_u\|^2 \le |S_1| + |S_2|.$$

Let us estimate S_1 and S_2. Applying Lemma 4.1 and Lemma 4.2 to Lemma 4.7, we get

$$\begin{aligned}S_1 = &- \varepsilon\langle \eta_u, \delta_\psi \boldsymbol{n}\rangle + \varepsilon\langle \eta_q, \delta_\varphi \boldsymbol{n}\rangle \\ &+ \varepsilon\langle (\delta_u + \eta_u)^- - \boldsymbol{i}\beta(\llbracket \delta_q \rrbracket + \llbracket \eta_q \rrbracket), \delta_\psi \boldsymbol{n}\rangle_{\partial\Omega_h \setminus \partial\Omega} \\ &- \varepsilon\langle (\delta_q + \eta_q)^+ + \boldsymbol{i}\alpha(\llbracket \delta_u \rrbracket + \llbracket \eta_u \rrbracket), \delta_\varphi \boldsymbol{n}\rangle_{\partial\Omega_h \setminus \partial\Omega} \\ &+ \varepsilon\langle (1-\gamma)(\delta_u + \eta_u) - \boldsymbol{i}\frac{\gamma}{\sqrt{f}}(\delta_q + \eta_q)\boldsymbol{n}, \delta_\psi \boldsymbol{n}\rangle_{\partial\Omega} \\ &- \varepsilon\langle \gamma(\delta_q + \eta_q) + \boldsymbol{i}(1-\gamma)\sqrt{f}(\delta_u + \eta_u)\boldsymbol{n}, \delta_\varphi \boldsymbol{n}\rangle_{\partial\Omega}\end{aligned}$$

After some algebraic manipulations, we have

$$\begin{aligned}
S_1 =& -\varepsilon\langle[\![\eta_u]\!],\delta_\psi^+ - \boldsymbol{i}\alpha[\![\delta_\varphi]\!]\rangle_{\mathscr{E}_h^i} + \varepsilon\langle[\![\eta_q]\!],\delta_\varphi^- + \boldsymbol{i}\beta[\![\delta_\varphi]\!]\rangle_{\mathscr{E}_h^i}\\
&-\varepsilon\langle\eta_u,(\gamma\delta_\psi - \boldsymbol{i}(1-\gamma)\sqrt{f}\delta_\varphi)\,\boldsymbol{n}\rangle_{\partial\Omega} + \varepsilon\langle\eta_q,((1-\gamma)\delta_\varphi + \boldsymbol{i}\frac{\gamma}{\sqrt{f}}\delta_\psi)\,\boldsymbol{n}\rangle_{\partial\Omega}\\
&+\varepsilon\langle\delta_u^- - \boldsymbol{i}\beta[\![\delta_q]\!],[\![\delta_\psi]\!]\rangle_{\mathscr{E}_h^i} - \varepsilon\langle\delta_q^+ + \boldsymbol{i}\alpha[\![\delta_u]\!],[\![\delta_\varphi]\!]\rangle_{\mathscr{E}_h^i}\\
&+\varepsilon\langle(1-\gamma)\delta_u - \boldsymbol{i}\frac{\gamma}{\sqrt{f}}\delta_q\,\boldsymbol{n},\delta_\psi\,\boldsymbol{n}\rangle_{\partial\Omega} - \varepsilon\langle\gamma\delta_q + \boldsymbol{i}(1-\gamma)\sqrt{f}\delta_u,\delta_\varphi\,\boldsymbol{n}\rangle_{\partial\Omega}.
\end{aligned}$$

Because $\alpha,\beta,\gamma,1-\gamma$ are positive constants, using the Cauchy's inequality, Lemma 3.2 and Lemma 4.6, we get

$$\begin{aligned}
|S_1| \le& C\varepsilon(\|[\![\eta_u]\!]\|_{\mathscr{E}_h} + \|[\![\eta_q]\!]\|_{\mathscr{E}_h})(\|\delta_\varphi\|_{\partial\Omega_h} + \|\delta_\psi\|_{\partial\Omega_h})\\
&+ C\varepsilon(\|\delta_u\|_{\partial\Omega_h} + \|\delta_q\|_{\partial\Omega_h})(\|\delta_\varphi\|_{\partial\Omega_h} + \|\delta_\psi\|_{\partial\Omega_h})\\
\le& C(h^{1/2} + \frac{h^{3/2}}{\varepsilon})(\|[\![\eta_u]\!]\|_{\mathscr{E}_h} + \|[\![\eta_q]\!]\|_{\mathscr{E}_h})\|\theta\| + C(\frac{h^2}{\varepsilon} + \frac{h^3}{\varepsilon^2})|f|_{1,\infty}\|u\|\|\theta\|.
\end{aligned}$$

Then by Theorem 3.3, we have

$$|S_1| \le C(\frac{h^2}{\varepsilon} + \frac{h^3}{\varepsilon^2})|f|_{1,\infty}\|\eta_u\|\|\theta\| + C(\frac{h^2}{\varepsilon} + \frac{h^3}{\varepsilon^2})|f|_{1,\infty}\|u\|\|\theta\|.$$

Similarly, we get

$$\begin{aligned}
|S_2| \le& \|f - \mathbb{P}^0 f\|_\infty\|\eta_u\|\|\delta\varphi\| + \|f - \mathbb{P}^0 f\|_\infty\|\delta_u\|\|\boldsymbol{\Pi}\varphi\|\\
\le& \|f - \mathbb{P}^0 f\|_\infty\|\eta_u\|\|\delta\varphi\| + \|f - \mathbb{P}^0 f\|_\infty\|\delta_u\|\|\varphi\|\\
\le& C(\frac{h^2}{\varepsilon} + \frac{h^3}{\varepsilon^2})|f|_{1,\infty}\|\eta_u\|\|\theta\| + C\frac{h^3}{\varepsilon^2}|f|_{1,\infty}\|u\|\|\theta\|.
\end{aligned}$$

So

$$\|\eta_u\|^2 \le C(\frac{h^2}{\varepsilon} + \frac{h^3}{\varepsilon^2})|f|_{1,\infty}\|\eta_u\|\|\theta\| + C(\frac{h^2}{\varepsilon} + \frac{h^3}{\varepsilon^2})|f|_{1,\infty}\|u\|\|\theta\|.$$

If $(\frac{h^2}{\varepsilon} + \frac{h^3}{\varepsilon^2})|f|_{1,\infty}$ is sufficiently small, we have

$$\|\eta_u\| \le C|f|_{1,\infty}(\frac{h^2}{\varepsilon} + \frac{h^3}{\varepsilon^2})\|u\|.$$

□

Table 5.1: Example 5.1: L^2-errors by multiscale DG with $\alpha = \beta = 1$, $\gamma = 0.5$.

N	$\varepsilon = 1$	$\varepsilon = 10^{-2}$	$\varepsilon = 10^{-3}$	$\varepsilon = 10^{-4}$
10	3.04E-15	9.74E-14	2.46E-11	9.42E-09
20	4.51E-15	8.14E-14	2.21E-11	9.00E-09
40	2.34E-14	1.39E-13	2.17E-11	2.13E-10
80	2.45E-14	1.45E-13	2.30E-11	2.32E-10

5 Numerical results by the multiscale DG

In this section, we will perform several numerical tests. The first example is to show the good approximation property of the multiscale bases E^1. The basis functions approximate the solution exactly when $f(x)$ is constant. The next example is to verify the second order convergence of our multiscale DG in the error estimates for a wide range of ε from 1 to 10^{-4}. In the last two examples, we apply the proposed scheme to the application of Schrödinger equation in the modeling of resonant tunneling diode (RTD).

For the proposed multiscale DG scheme, we use $\alpha = \beta = 1$ and $\gamma = 0.5$ in the tests. For other constants α, β and $0 < \gamma < 1$, the numerical results are similar and thus we do not show them here. When $\alpha = \beta = \gamma = 0$, the method becomes the minimal dissipation LDG (MD-LDG) method [8] with multiscale basis E^1. Although our analysis does not cover this case, numerically we see a similar second order convergence.

5.1 Constant f

Example 5.1. In the first example, we consider the simple case with constant function $f(x)$. When $f(x)$ is a constant, the exact solution of (2.1) is in the finite element space E^1. Thus the multiscale DG method can compute the solution exactly with only round off errors. The L^2-errors of the multiscale DG with $\alpha = \beta = 1$ and $\gamma = 0.5$ for the case $f(x) = 10$ are shown in Table 5.1. It is clear to see the round-off errors (in double precision) for ε ranging from 1 to 10^{-4}. We remark that when ε is small, numerically integrating the exponential functions accumulates round-off errors. Thus the errors increase when ε becomes small .

5.2 Accuracy test

Example 5.2. In this example, we consider a smooth function $f(x) = \sin x + 2$. Table 5.2 lists the L^2-errors and orders of accuracy by the proposed multiscale DG scheme with $\alpha = \beta = 1$, $\gamma = 0.5$ for ε from 1 to 10^{-4}. The reference solutions are computed by polynomial-based MD-LDG P^3 method with $N = 50,000$ cells for $\varepsilon = 1$ and with $N = 500,000$ for $\varepsilon = 10^{-2}, 10^{-3}, 10^{-4}$. Note that we stop refining the mesh when the errors are smaller than 10^{-8}. We can see a clean second order convergence for both $h > \varepsilon$ and $h < \varepsilon$. For the same h, when ε decreases to one tenth, the magnitude of the error increases by ten times. This verifies the convergence order is of $O(h^2/\varepsilon)$ in Theorem 3.4.

We also show the results by the multiscale MD-LDG method with E^1 space, i.e. the proposed multiscale DG method with $\alpha = \beta = \gamma = 0$, in Table 5.3. Although our analysis is inconclusive in this case, we observe a second order convergence when $h > \varepsilon$ and a third order convergence when $h < \varepsilon$.

Next, we compare the results with the WKB-LDG method in [18] in Table 5.4. Note that WKB-LDG method is the multiscale MD-LDG method with E^2 space, which has one more basis function "1" than the E^1 space. Similar to the MD-LDG method with E^1 space, MD-LDG method with E^2 space also has a second order convergence when $h > \varepsilon$ and a third order convergence when $h < \varepsilon$. However, we observe a resonance error around $h = \varepsilon$ whereas our new proposed multiscale schemes do not have it. In Table 5.5, we show the condition numbers of the global matrices for the WKB-LDG method with E^2 space and our proposed DG method with E^1 space. Note that the condition numbers by using E^2 space become very large when $N = 20$ for $\varepsilon = 10^{-2}$ and when $N = 160$ for $\varepsilon = 10^{-3}$. Those are exactly where the resonance errors are observed in Table 5.4. In contrast, the condition numbers by using E^1 space only change slightly. This shows why removing the basis function "1" from the finite element basis will reduce the resonance errors.

At the end of this section, we compare our multiscale DG with the MD-LDG using polynomials P^1 and P^2 in Table 5.6. Standard DG methods using polynomials do not have any order of convergence until the mesh is refined to $h < \varepsilon$. For example, for $\varepsilon = 10^{-2}$, MD-LDG P^1 shows a second order starting from $N = 160$ and MD-LDG P^2 shows a third order starting from $N = 80$. When ε becomes even smaller to 10^{-3}, for both P^1 and P^2, there is no order of convergence till $N = 640$. The multiscale DG method is convergent when

Table 5.2: Example 5.2: L^2-errors and orders of accuracy by multiscale DG with $\alpha = \beta = 1$, $\gamma = 0.5$.

	$\varepsilon = 1$		$\varepsilon = 10^{-2}$		$\varepsilon = 10^{-3}$		$\varepsilon = 10^{-4}$	
N	error	order	error	order	error	order	error	order
10	1.62E-04	–	2.56E-02	–	2.47E-01	–	1.56	–
20	3.95E-05	2.04	7.08E-03	1.85	6.27E-02	1.98	6.09E-01	1.36
40	9.75E-06	2.02	2.50E-03	1.50	1.58E-02	1.98	1.57E-01	1.95
80	2.42E-06	2.01	4.37E-04	2.52	4.03E-03	1.97	3.95E-02	1.99
160	6.04E-07	2.00	7.17E-05	2.61	1.09E-03	1.88	9.89E-03	2.00
320	1.51E-07	2.00	1.60E-05	2.17	3.06E-04	1.83	2.48E-03	1.99
640	3.81E-08	1.99	3.89E-06	2.04	8.52E-05	1.84	6.30E-04	1.98
1280	–	–	1.00E-06	1.96	1.22E-05	2.81	1.62E-04	1.96

h is much larger than ε, and when $h < \varepsilon$, it also approximates the problem much more accurately than the standard DG. For example, when $\varepsilon = 10^{-2}$ and $N = 640$, the error is $O(10^{-3})$ by using P^1, $O(10^{-5})$ by P^2, and $O(10^{-7})$ by E^1. Therefore, the multiscale DG is more efficient and accurate than the standard DG methods for solving the stationary Schrödinger equation.

5.3 Applications to Schrödinger equation

In this section, we apply our proposed multiscale DG method to solve the Schrödinger equation in the simulation of the resonant tunneling diode (RTD) model. RTD model is used to collect the electrons which have an energy extremely close to the resonant energy.

We consider the RTD model (see [5]) on the interval $[0, 135nm]$. Its conduction band profile consists of two barriers of height $-0.3v$ located at $[60, 65]$ and $[70, 75]$. A bias energy $\triangle v$ is applied between the source and the collector regions.

The wave function of the electrons injected at $x = 0$ with an energy $E > 0$ satisfies the stationary Schrödinger equation with open boundary conditions, (1.2), with $m = 0.067m_e$. In our numerical simulations, we consider the total potential to be the external potential only. Figure 5.1 shows the external potential with the double barriers and an applied bias. These numerical tests were also performed in [5, 18].

Table 5.3: Example 5.2: L^2-errors and orders of accuracy by multiscale DG with $\alpha = \beta = 0$, $\gamma = 0$.

	$\varepsilon = 1$		$\varepsilon = 10^{-2}$		$\varepsilon = 10^{-3}$		$\varepsilon = 10^{-4}$	
N	error	order	error	order	error	order	error	order
10	1.01E-05	–	2.54E-02	–	2.52E-01	–	1.58E-00	–
20	1.42E-06	2.95	9.48E-03	1.42	6.34E-02	1.99	6.20E-01	1.35
40	1.79E-07	2.99	2.30E-03	2.05	1.59E-02	2.00	1.59E-01	1.96
80	2.23E-08	3.00	2.74E-04	3.07	3.98E-03	2.00	3.96E-02	2.01
160	–	–	3.05E-05	3.17	1.01E-03	1.98	9.90E-03	2.00
320	–	–	3.68E-06	3.05	2.84E-04	1.83	2.48E-03	2.00
640	–	–	4.56E-07	3.01	5.58E-05	2.34	6.33E-04	1.97

Table 5.4: Example 5.2: L^2-errors and orders of accuracy by WKB-LDG in [18].

	$\varepsilon = 1$		$\varepsilon = 10^{-2}$		$\varepsilon = 10^{-3}$		$\varepsilon = 10^{-4}$	
N	error	order	error	order	error	order	error	order
10	4.02E-06	–	2.54E-2	–	2.52E-01	–	1.58E-00	–
20	5.70E-07	2.82	5.70E-02	-1.17	6.58E-02	1.94	6.21E-01	1.35
40	–	–	5.51E-04	6.69	1.58E-02	2.06	1.58E-01	1.97
80	–	–	7.43E-05	2.89	3.89E-03	2.02	3.96E-02	2.00
160	–	–	9.63E-06	2.95	7.56E-03	-0.96	9.90E-03	2.00
320	–	–	1.21E-06	2.99	1.16E-04	6.03	3.68E-03	1.43
640	–	–	1.55E-07	2.97	1.41E-05	3.04	7.13E-04	2.37

Table 5.5: Example 5.2: Condition numbers of the global matrices (in L^∞ norm) by the proposed scheme with E^1 space and WKB-LDG with E^2 space.

	$\varepsilon = 10^{-2}$		$\varepsilon = 10^{-3}$	
N	E^1	E^2	E^1	E^2
10	6.54E+02	9.80E+02	6.05E+03	7.56E+03
20	7.64E+02	1.39E+04	6.17E+03	7.03E+04
40	9.83E+02	1.11E+03	6.43E+03	6.97E+03
80	1.44E+03	2.63E+03	6.34E+03	1.20E+04
160	2.66E+03	4.42E+04	7.15E+03	1.21E+05
320	5.26E+03	1.11E+06	9.70E+03	9.62E+03
640	1.01E+04	3.24E+07	1.29E+04	1.40E+04

Table 5.6: Example 5.2: L^2-errors and orders of accuracy by standard MD-LDG P^1 and P^2.

	P^1				P^2			
	$\varepsilon = 10^{-2}$		$\varepsilon = 10^{-3}$		$\varepsilon = 10^{-2}$		$\varepsilon = 10^{-3}$	
N	error	order	error	order	error	order	error	order
10	9.53E-01	–	9.51E-01	–	9.47E-01	–	9.51E-01	–
20	9.60E-01	-0.01	9.51E-01	0.00	9.55E-01	-0.01	9.51E-01	0.00
40	9.51E-01	0.01	9.51E-01	0.00	4.46E-01	1.10	9.51E-01	0.00
80	1.17E-00	-0.29	9.51E-01	0.00	3.92E-02	3.51	9.52E-01	0.00
160	7.88E-02	3.89	9.52E-01	0.00	4.42E-03	3.15	9.53E-01	0.00
320	1.42E-02	2.47	9.57E-01	-0.01	5.51E-04	3.00	2.05E-00	-1.11
640	3.49E-03	2.02	2.08E-00	-1.12	6.88E-05	3.00	7.72E-01	1.41

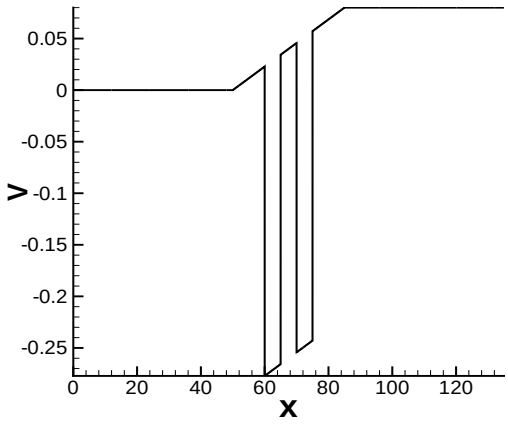

Figure 5.1: External voltage with double barriers of height $-0.3v$ located at $[60, 65]$ and $[70, 75]$ and an applied bias of $0.8V$.

Example 5.3. In the first application example, we consider the energy $E = 0.0895eV$ which is very close to the double-barrier resonant energy. For simplicity, no bias is applied to the external potential and the potential function $V(x)$ is a piecewise constant function

$$V(x) = \begin{cases} 0, & x < 60 \\ -0.3, & 60 < x < 65 \\ 0, & 65 < x < 70 \\ -0.3, & 70 < x < 75 \\ 0, & x > 75 \end{cases}.$$

In this case, our proposed multiscale DG method can approximate the solution exactly with round off errors. We only use 23 cells for the proposed multiscale DG method with 6 cells each in $[0, 50]$, $[85, 135]$, 2 cells each in $[50, 60]$, $[60, 65]$, $[70, 75]$ and $[75, 85]$, and 3 cells in $[65, 70]$.

Figure 5.2 shows the wave function modulus for the case of the resonance energy $E = 0.0895eV$. We see a big spike in the double barriers area [60,75]. The proposed multiscale DG method is able to capture the resonance spike in only 23 cells. The standard polynomial-based DG methods will need a much more refined mesh to capture the resonance.

Example 5.4. In the next example, a bias of $0.08V$ is added at the edges of the device. We compute in the case of a very high energy $E = 1.11eV$ and

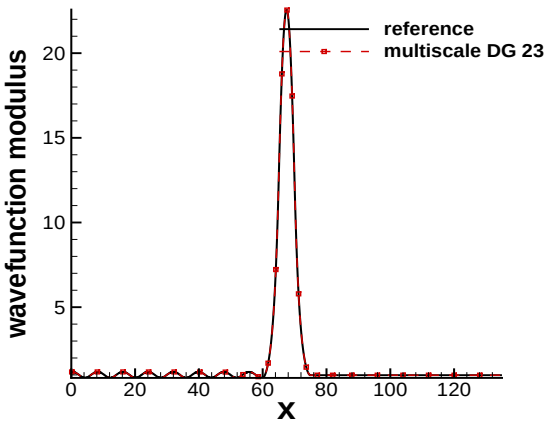

Figure 5.2: Wavefunction modulus by multiscale DG for the resonance energy $E = 0.0895eV$. 23 cells are used in the multiscale DG method. In each cell, the solution is plotted as a function using 27 points.

the solution will be highly oscillating. The reference solution was obtained by the polynomial-based MD-LDG P^3 method of 13,500 cells. Figure 5.3 shows the wave function modulus computed by the multiscale DG with 23 cells. In each cell, the solution is plotted as a function using 27 points. We can see although the solution is highly oscillating, the proposed scheme matches the reference solution very well. The L^2-error is 1.49×10^{-5}. The standard polynomial-based DG methods cannot well approximate the solution unless the mesh is very refined.

6 Concluding remarks

In this paper, we have developed a new multiscale discontinuous Galerkin method for a special second order elliptic equation with applications to one-dimensional stationary Schrödinger equations. The basis functions are constructed based on the WKB asymptotic and thus have good approximations to the solutions. The error estimate shows a second order convergent rate for both $h \gtrsim \varepsilon$ and $h \lesssim \varepsilon$. Numerical experiments confirmed the convergent rate and also demonstrated excellent accuracy on very coarse meshes when applied to Schrödinger equations. Compared with the continuous finite element

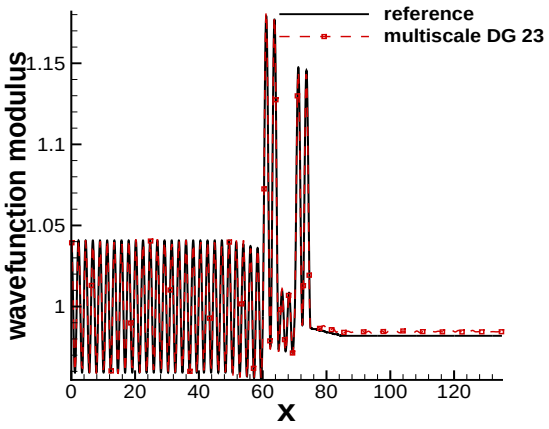

Figure 5.3: Wavefunction modulus by the multiscale DG for a high energy $E = 1.11eV$. 23 cells are used in the multiscale DG method. In each cell, the solution is plotted as a function using 27 points.

based WKB method in [5], the multiscale DG method allows the full usage of the potential of this methodology in easy h-p adaptivity and feasibility for the extension to two-dimensional case. Compared with the WKB-LDG method in [18], the new multiscale DG method uses a smaller finite element space and more importantly, it dose not have resonance errors. In future work, we will generalize our multiscale DG method to two-dimensional Schrödinger equations.

7 Compliance with Ethical Standards

The authors consent to comply with all the Publication Ethical Standards. The research of the first author is supported by NSF grant DMS-1419029. The research of the second author is supported by DOE grant DE-FG02-08ER25863 and NSF grant DMS-1418750. The research of the third author is supported by NSF grant DMS-1418953.

References

[1] J. Aarnes and B.-O. Heimsund, *Multiscale discontinuous Galerkin methods for elliptic problems with multiple scales*, Multiscale methods in science and engineering 1–20, Lect. Notes Comput. Sci. Eng., 44. Springer, Berlin, 2005.

[2] D.N. Arnold, F. Brezzi, B. Cockburn and L.D. Marini, *Unified analysis of discontinuous Galerkin methods for elliptic problems*, SIAM J. Numer. Anal., **39**, 2002, 1749–1779.

[3] A. Arnold, N Ben Abdallah and C. Negulescu, WKB-based schemes for the oscillatory 1D Schrödinger equation in the semiclassical limit, SIAM J. Numer. Anal., 49, 2011, 1436–1460.

[4] N. Ben Abdallah, M. Mouis and C. Negulescu, *An accelerated algorithm for 2D simulations of the quantum ballistic transport in nanoscale MOSFETs*, J. Comput. Phys., **225**, 2007, 74–99.

[5] N. Ben Abdallah and O. Pinaud, *Multiscale simulation of transport in an open quantum system: Resonances and WKB interpolation*, J. Comput. Phys., **213**, 2006, 288–310.

[6] D. Bohm, *Quantum Theory*, Dover, New York, 1989.

[7] A. Buffa and P. Monk, *Error estimates for the Ultra Weak Variational Formulation of the Helmholtz equation*, ESAIM: M2AN Math. Model. Numer. Anal. **42**, 2008, 925–940.

[8] B. Cockburn and B. Dong, *An analysis of the minimal dissipation local discontinuous Galerkin method for convection-diffusion problems*, J. Sci. Comput., **32**, 2007, 233–262.

[9] B. Cockburn and C.-W. Shu, *Runge-Kutta discontinuous Galerkin methods for convection-dominated problems*, J. Sci. Comput., **16**, 2001, 173–261.

[10] X. Feng and H. Wu, *Discontinuous Galerkin methods for the Helmholtz equation with large wave number*, SIAM J. Numer. Anal., **47**, 2009, 2872–2896.

[11] G. Gabard, *Discontinuous Galerkin methods with plane waves for time-harmonic problems*, J. Comput. Phys., **225**, 2007, 1961–1984.

[12] C. Gittelson, R. Hiptmair, and I. Perugia, *Plane wave discontinuous Galerkin methods: Analysis of the h-version*, ESAIM: M2AN Math. Model. Numer. Anal., **43**, 2009, 297–331.

[13] C. S. Lent and D. J. Kirkner, *The quantum transmitting boundary method*, J. Appl. Phys. **67**, 1990, 6353–6359.

[14] C. Negulescu, *Numerical analysis of a multiscale finite element scheme for the resolution of the stationary Schrödinger equation*, Numer. Math., **108**, 2008, 625–652.

[15] C. Negulescu, N. Ben Abdallah, E. Polizzi and M. Mouis, *Simulation schemes in 2D nanoscale MOSFETs: A WKB based method*, J. Comput. Electron., **3**, 2004, 397–400.

[16] E. Polizzi and N. Ben Abdallah, *Subband decomposition approach for the simulation of quantum electron transport in nanostructures*, J. Comput. Phys., **202**, 2005, 150–180.

[17] W. Wang, J. Guzmán and C.-W. Shu, *The multiscale discontinuous Galerkin method for solving a class of second order elliptic problems with rough coefficients*, Int. J. Numer. Anal. Model, **8**, 2011, 28–47.

[18] W. Wang and C.-W. Shu, *The WKB local discontinuous Galerkin method for the simulation of Schrödinger equation in a resonant tunneling diode*, J. Sci. Comput., **40**, 2009, 360–374.

[19] L. Yuan and C.-W. Shu, *Discontinuous Galerkin method based on non-polynomial approximation spaces*, J. Comput. Phys., **218**, 2006, 295–323.

[20] L. Yuan and C.-W. Shu, *Discontinuous Galerkin method for a class of elliptic multi-scale problems*, Int. J. Numer. Meth. Fluids, **56**, 2008, 1017–1032.

[21] Y. Zhang, W. Wang, J. Guzmán and C.-W. Shu, *Multi-scale discontinuous Galerkin method for solving elliptic problems with curvilinear unidirectional rough coefficients*, J. Sci. Comput., **61**, 2014, 42–60.